Comparative study of a concentrated photovoltaic-thermoelectric system with and without flat plate heat pipe

Samson Shittu

Guiqiang Li*

Guiqiang.Li@hull.ac.uk

Xudong Zhao*

Xudong.Zhao@hull.ac.uk

Yousef Golizadeh Akhlaghi

Xiaoli Ma

Min Yu

School of Engineering and Computer Science, University of Hull, HU6 7RX, UK

*Corresponding authors.

Abstract

Thermal management of photovoltaic cells is an essential research objective for increasing the conversion efficiency of the photovoltaic. Flat plate heat pipe is a passive cooling device capable of effectively reducing the solar cell temperature. Therefore, this study presents a numerical investigation of a hybrid photovoltaic-thermoelectric system with and without a flat plate heat pipe. A detailed comparative analysis of the electrical performance of the photovoltaic only, photovoltaic-thermoelectric and photovoltaic-thermoelectric-heat pipe systems is performed. The influence of solar concentration ratio, ambient temperature, wind speed and thermoelectric generator cold side temperature on the efficiency and power output of the photovoltaic only and hybrid photovoltaic-thermoelectric systems are studied using COMSOL 5.4 Multiphysics software. A three-dimensional finite element study is carried out and temperature dependent thermoelectric material properties are considered to increase the simulation accuracy. Results show that the photovoltaic-thermoelectric-heat pipe efficiency is 1.47% and 61.01% higher compared to that of the photovoltaic-thermoelectric and photovoltaic only systems respectively at a concentration ratio of 6. In addition, the photovoltaic-thermoelectric-heat pipe is recommended for highly concentrated systems because of its superior performance. Furthermore, the photovoltaic-thermoelectric system is a better alternative to the photovoltaic only system because of its enhanced performance which is second only to that of the photovoltaic-thermoelectric-heat pipe system. Results also show that ineffective cooling of the thermoelectric generator can adversely affect the performance of the hybrid systems. This study will proper valuable information on the feasibility of hybrid photovoltaic-thermoelectric systems with and without heat pipe. Finally, the three-dimensional nature of this study makes it very useful in understanding the actual temperature distribution in the hybrid systems.

Keywords: Photovoltaic-thermoelectric; PV; Heat pipe; Thermal management; Finite element method

Nomenclature

C

concentration ratio

C_P

specific heat capacity, J/kg/K

G

solar irradiance, W/m^2

h

convective heat transfer coefficient, W/m^2/K

h_{fg}

latent heat, kJ/kg

I

current, A

M_n

molar mass, g/mol

P

power output, W

$\dot{P}$

power generated per volume, W/m^3

p_c

capillary pressure, Pa

p_g

gravitational pressure

p_l

liquid pressure, Pa

p_{sat}

saturation pressure, Pa

p_v

vapor pressure, Pa

$\dot{q}$

volumetric energy absorption, W/m^3

ρ_v

vapor density, kg/m^3

R_{in}

internal resistance, Ω

R_L

load resistance, Ω

R_s

specific gas constant, J/mol/K

T

temperature, K

Z

figure of merit, K^{-1}

Greek symbols

$α$

Seebeck coefficient, V/K

$η$

efficiency

$σ$

electrical conductivity, S/m

$κ$

thermal conductivity, W/m/K

$ρ$

density, Kg/m^3

$β$

PV temperature coefficient, K^{-1}

Abbreviations

AM

air mass

Bi_2Te_3

bismuth telluride

EVA

ethylene vinyl acetate

PV

photovoltaic

PV-TE

photovoltaic-thermoelectric

TE

thermoelectric

TEG

thermoelectric generator

TPT

Tedlar polyester tedlar

Subscripts

A

ambient

c

solar cell

sky

sky

1 Introduction

The current increased energy demand necessitates the need for renewable energy sources like solar energy which is a feasible and long-term solution to the global energy crisis because it is clean, renewable and environmentally-friendly [1]. Solar energy can be easily harnessed in two forms; electrical and thermal energy. Photovoltaic (PV) can be used to directly convert solar radiations to electrical energy while thermoelectric generator can be used to convert thermal energy into electrical energy [2]. The PV mainly converts the ultraviolent and visible regions of the solar spectrum while the thermoelectric (TE) utilizes the infrared region therefore, combining the photovoltaic and thermoelectric effects can potentially lead to a wider utilization of the solar spectrum [3]. Presently, the PV technology is one of the attractive solutions which can increase the share of used renewable energy and possess a potential to deliver around 5% of the global electricity demand by 2030 and 11% by 2050 [4]. Although the PV technology has immerse potential, its wide application has been hindered by key issues such as: limited conversion efficiency, elevated temperatures and dust accumulation [5]. To increase the electrical efficiency of PV and efficiently utilize the incident solar radiation, it is imperative to remove the accumulated heat from the PV surface and utilize this waste heat appropriately [6].

Thermoelectric devices can be used for cooling, heating and micro-power generation because they offer some distinct advantages over other technologies [7]. A thermoelectric generator (TEG) is a solid-state heat engine capable of producing electrical energy from heat via the Seebeck effect when a temperature gradient is present across its thermoelements [8]. The thermoelectric generator offers several advantages such as: simple design, small size, no moving parts, high reliability and environmentally friendly [9]. Despite all these advantages that the TEG offers, its application is limited mainly because of its low energy conversion efficiency and high material cost. Therefore, the majority of research on thermoelectric generator is based on increasing its conversion efficiency and reducing the material cost so as to increase its widespread application [10]. In theory, the efficiency and power output of a TEG can be enhanced by increasing the temperature difference across its thermoelements. This can be achieved by either increasing the solar concentration on the TEG or by effectively cooling the TEG. Machrafi [11] developed an analytical mathematical model for a cooled hybrid photovoltaic-thermoelectric system in which the photovoltaic device powered the cooling system and an enhanced overall efficiency was observed. Similarly, Hashim et al. [12] presented a model for photovoltaic cooling with the use of thermoelectric generators. A numerical study was performed to optimize the system for obtaining maximum power output and results showed that the incorporation of TEG into PV led to an increase in overall power output and conversion efficiency of the hybrid system.

Heat pipes are efficient heat transfer device which can be used to cool electronic devices. Currently, there are several ways to cool electronic devices such as natural convection, forced air cooling, micro-channel cooling and phase change material. However, each one of them have well known disadvantages such as: inefficiency, need for pump, valve, low thermal conductivity and low reliability [13]. Heat pipe is a vapor-liquid phase change equipment that offer advantages such as: absence of moving parts [14], compact structure, high heat transfer under small temperature gradient with little heat loss [15]. The disadvantage of using the heat pipe is that the overall system cost would be increased, and the system design might be complicated. In addition, there are five primary heat pipe

transport limitations that have to be considered during design including, continuum flow limit, sonic limit, capillary limit, entrainment limit, viscous limit and boiling limit [16]. While active cooling methods like forced air cooling require the use of electricity which results in increased energy consumption, reduced overall electrical power output and increased system costs, passive cooling methods like heat pipe do not use any electricity therefore, no energy input is required and the overall electrical power and efficiency are not affected.

Research on hybrid photovoltaic-thermoelectric (PV-TE) has increased exponentially in recent times due to the great level of interest in this field. Generally, the design of PV-TE can be divided into spectrum splitting design and direct coupling design. Ju et al. [17] presented a numerical investigation of a spectrum splitting PV-TE hybrid system. Results obtained showed that the cut-off wavelength of the hybrid PV-TE system was determined by the band gap of the solar cell. Yin et al. [18] presented a novel optimal design method for a concentrated spectrum splitting photovoltaic-thermoelectric hybrid system. They found that the optimum cut-off wavelength of the spectral splitter decreases with the increase of the thermoelectric figure of merit.

In terms of the direct coupling design, van Sark [19] performed a feasibility study on a PV-TE system for two cities (Malaga, Spain and Utrecht, Netherlands). Results showed that when thermoelectric materials with typical figure of merit value of 0.004 K^{-1} at 300 K were used, a 23% increase in efficiency was obtained from the roof integrated PV-TE system using an idealized model calculation. Li et al. [20] studied the inconsistent phenomenon of thermoelectric load resistance in a hybrid PV-TE system. Results showed that the optimum thermoelectric load resistance for maximum power output in a TE only, TE in PV-TE and PV-TE are all different.

Furthermore, Zhang et al. [21] introduced a new concept for an integrated design of a hybrid PV-TE system in which ceramic plates of the thermoelectric modules are eliminated from the hybrid system to enhance the heat transfer in the system and reduce the thermal resistance. Results showed that the simplified TE structure enhanced the efficiency of both the PV and the TEG. Lekbir et al. [22] presented another feasibility study of a hybrid PV-TE system. The experimental results showed that the maximum resistive output power of the hybrid system was about 0.12 W which was 75% greater than that of the PV cell and TEG. Rodrigo et al. [23] presented a detailed analysis of the performance of a passively cooled hybrid CPV-TE system. They argued that the use of simple and reliable passive cooling could accelerate the development of new hybrid PV-TE systems. Recently, Mahmoudinezhad et al. [24] performed an experimental and numerical investigation of the transient behaviour of a hybrid concentrating triple junction solar cell thermoelectric generator system. Results obtained showed that the use of TEG in a hybrid system allowed for the achievement of a more stable overall output power rather than a fluctuating power output.

Heat pipes which are passive cooling devices have been introduced into the hybrid PV-TE system design to potentially enhance the performance of the hybrid system. Makki et al. [25] theoretically studied a hybrid PV-TE system integrated with a heat pipe. Results obtained showed that the hybrid system was favourable for sunny regions with high operating temperature and low wind speeds. Similarly, Li et al. [26] presented a novel design for a hybrid PV-TE system integrated with a flat-plate micro-channel heat pipe. Results obtained showed that the new PV-TE system with flat plate heat pipe provided a higher electronical output and economic performance compared to the conventional PV only system. Finite element method is an effective numerical simulation approach for studying hybrid PV-TE systems [27]. Shittu et al. [28] investigated the optimum geometry of a TE in a hybrid PV-TE system using finite element method. Results obtained showed that the performance of the hybrid PV-TEG system is dependent on the geometry of the TEG and the temperature coefficient value of the PV used. This finding was in agreement with Li et al. [29] who also emphasised the need for thermoelectric geometry optimization.

Presently, there are very few studies on the three-dimensional investigation of a hybrid PV-TE system. Recently, Fallah Kohan et al. [30] presented such a study and only two papers Li et al. [25], Makki et al. [26] have attempted to investigate the potential of a hybrid PV-TE system with a heat pipe. However, in [30], temperature dependent thermoelectric material properties were not used and only the hybrid PV-TE system without heat pipe was investigated. Furthermore, in both [25] and [26] only a one-dimensional numerical study was carried rather than a three-dimensional study on the PV-TE system with heat pipe. The power output and efficiency of a TEG is affected by its temperature dependent thermoelectric material properties [31] therefore, it is very important to consider the temperature dependency of the TE materials during simulation to increase the accuracy of the results obtained [32]. In addition, a three-dimensional numerical study would provide a more realistic simulation with reduced deviation from the actual reality. The resulting three-dimensional temperature distribution in the hybrid system would facilitate the understanding of heat transfer process in the system and enhance the performance predictions.

Therefore, in this paper, for the first time, a three-dimensional numerical investigation of a hybrid PV-TE system with and without flat-plate heat pipe is presented and compared to a conventional PV only system under varying ambient conditions. COMSOL 5.4 Multiphysics simulation software is used to perform all the numerical simulations and temperature dependent thermoelectric material properties are accounted for. The remainder of this paper is organized as follows: Section 2 presents a detailed description of the PV, PV-TE and PV-TE-Heat pipe structures and materials used in this study, Section 3 presents the numerical model for each of the subsystems (PV, TEG, Heat pipe) and that of the hybrid system while Section 4 shows the results obtained and corresponding discussion. Finally, Section 5 presents the conclusions from this study.

2 Structure description and material properties

The structure of each of the systems studied in this paper is shown in Fig. 1. The schematic of the PV only can be seen in Fig. 1a. A typical polycrystalline silicon photovoltaic cell consists of five layers namely: glass, ethylene vinyl acetate (EVA), polycrystalline silicon cell, EVA and TPT (tedlar polyester tedlar) from top to bottom respectively as shown in Fig. 1a. All the layers of the PV are assumed to be of equal dimension of 40 mm × 40 mm. The top glass cover is used to provide mechanical strength and rigidity with low reflection and high transmission of light. The EVA is an encapsulant used to provide adhesion between the solar cell, the top surface and the back layer (TPT) of the PV. The solar cell is used to convert solar radiations to electricity directly via the photovoltaic effect while the tedlar is used to provide back surface protection. The hybrid PV-TE system studied is designed using the direct coupling PV-TE design. Therefore, the TEG module is attached directly to the back of the PV as shown in Fig. 1b. The dimension of the TEG module is 40 mm × 40 mm with 128 p and n thermoelectric legs and it is attached to the back of the PV. A thermoelectric generator (TEG) module is composed of the following layers: ceramic, copper and semiconductor thermoelectric materials. The ceramic layers are present at the top and bottom surface of the TEG and it provides thermal conductivity while the copper layers provide the electrical connection in the TEG and the thermoelectric legs are made of n-type and p-type thermoelectric materials. A three-dimensional schematic diagram of the hybrid PV-TE-Heat pipe system studied in this paper is shown in Fig. 1c. The PV is attached directly to the evaporator section of the flat plate heat pipe while the TEG is attached to the bottom surface of the heat pipe condenser section. The dimensions of the evaporator

section of the heat pipe are exactly the same with that of the PV (40 mm × 40 mm) while the dimensions of the condenser section of the heat pipe is the same with that of the TEG (40 mm × 40 mm). The flat plate heat pipe consists of a solid container, wick and vapor chamber as shown in Fig. 1d. The geometric parameters used in this study are listed in Table 1.
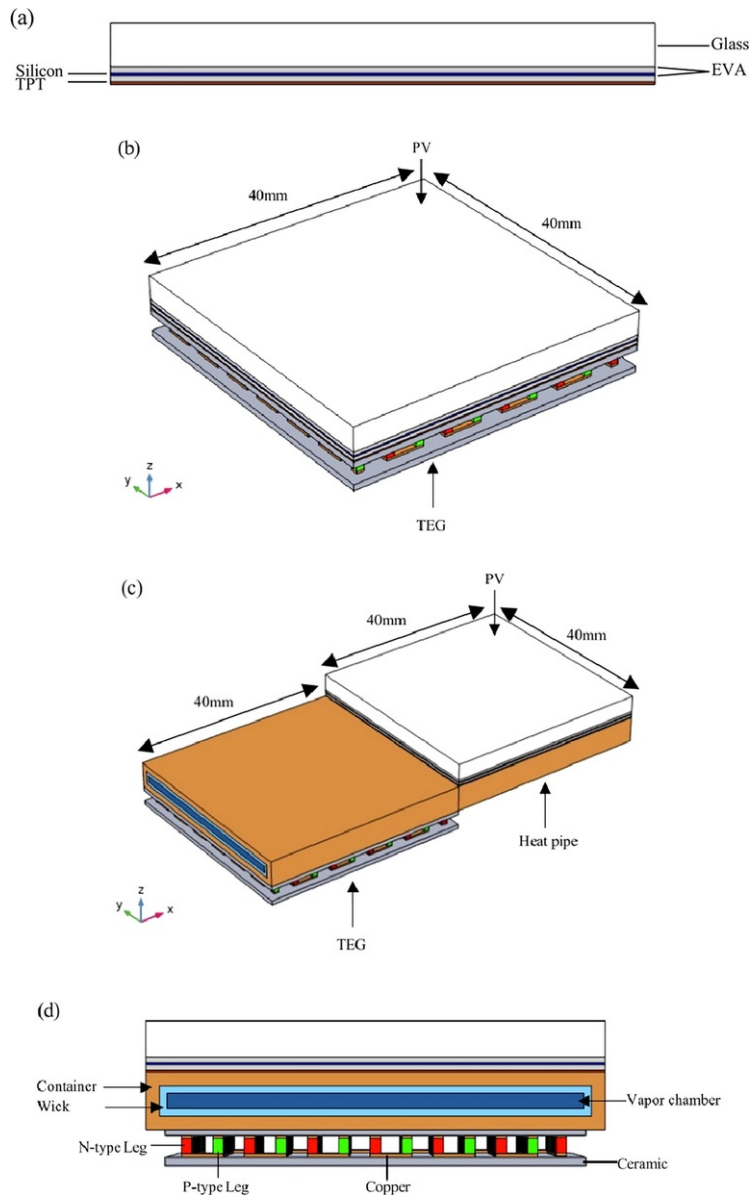
Fig. 1 Schematic diagram of (a) PV front view (b) three dimensional PV-TE (c) three dimensional PV-TE-Heat pipe (d) PV-TE-Heat pipe side view.

Table 1 Geometric parameters used in simulation [34,43].

Parameter	Value

PV	
Area	40 mm × 40 mm
Glass thickness	3.20 mm
EVA thickness	4.60×10^{-1} mm
Polycrystalline silicon thickness	1.80×10^{-1} mm
Tedlar/PET/Tedlar thickness	1.80×10^{-1} mm
TEG	
Area	40 mm × 40 mm
Leg area	1 mm × 1 mm
Leg thickness	1.5 mm
Copper thickness	0.3 mm
Ceramic thickness	0.8 mm
Heat pipe	
Evaporator	40 mm × 40 mm
Condenser	40 mm × 40 mm
Thickness	5 mm

2.1 System operation description

The operation of the hybrid PV-TE system is quite simple in that, the solar radiation is impinged on the PV surface after concentration by a solar concentrator. The radiation is then transmitted via each of the PV layers and some part is converted directly into electricity by the polycrystalline silicon cell while some other part is lost to the environment by radiation and convection. The remaining heat is transferred to the attached TEG module via conduction thereby providing the input heat flux needed for the TEG. The TEG cold side is attached to a cooling base and a fixed temperature boundary condition is used to model the cold side temperature. Therefore, a temperature gradient is produced in the TEG and electrical energy is generated via the Seebeck effect. Considering the PV-TE-Heat pipe, the PV is attached to the upper surface of the flat plate heat pipe evaporator while the TEG is attached to the lower surface of the condenser. When the hybrid system is being operated, solar radiation is impinged on the upper surface of the PV modules which are attached to the flat plate evaporator. The heat input vaporizes the working fluid in liquid form at the wick surface in the evaporator section and then the vapor and its latent heat flow towards the colder condenser section. In the condenser section, heat is released via condensation of the heat pipe working fluid and this heat is transferred to the attached TEG. Subsequently, thermal energy is converted into electrical energy by the TEG via the Seebeck effect. The back surface of the heat pipe is assumed to be insulated (no heat loss) so as to create enough temperature difference across the attached thermoelectric generator.

2.2 Material properties

The equations for the temperature dependent thermoelectric material properties of Bismuth telluride (Bi_2Te_3) used in this study are shown in Table 2. Bismuth telluride is chosen because it is the best performing thermoelectric material for low temperature range (<500 K). The optical properties of the PV layers are shown in Table 3 while the remaining material properties used in this study are shown in Table 4. In the heat pipe, user-defined constant vapour material properties are used in the vapor chamber while user-defined constant water material properties are used in the wick and copper material is used for the solid container.

Table 2 Temperature dependent thermoelectric material properties (T is temperature in K) [44].

	p-type	n-type
Electrical conductivity, $\sigma[S/m]$	$(0.015601732\ T^2 - 15.708052\ T + 4466.38095) \times 10^2$	$(0.01057143\ T^2 - 10.16048\ T + 3113.714229) \times 10^2$

Seebeck coefficient, $S[V/K]$	$(-0.003638095\, T^2 + 2.74380952\, T - 296.214286) \times 10^{-6}$	$(0.00153073\, T^2 - 1.08058874\, T - 28.338095) \times 10^{-6}$
Thermal conductivity, $k\,[W/(m \cdot K)]$	$0.0000361558\, T^2 - 0.026351342\, T + 6.22162$	$0.0000334545\, T^2 - 0.023350303\, T + 5.606333$

Table 3 Optical properties of PV materials [34].

Material	Reflectivity	Absorptivity	Transmissivity	Emissivity
Glass	4.00×10^{-2}	4.00×10^{-2}	9.20×10^{-1}	8.50×10^{-1}
EVA	2.00×10^{-2}	8.00×10^{-2}	9.00×10^{-1}	
Polycrystalline silicon	8.00×10^{-2}	9.00×10^{-1}	2.00×10^{-2}	
TPT	8.60×10^{-1}	1.28×10^{-1}	1.20×10^{-2}	9.20×10^{-1}

Table 4 Remaining material properties used for simulation [28,34,41].

	Heat capacity, C_p [J/(kgK)]	Density, ρ [kg/m3]	Seebeck coefficient, S [V/K]	Electrical conductivity, σ [S/m]	Thermal conductivity, k [W/(mK)]	Dynamic viscosity, mu [Pa·s]
Glass	5×10^2	2.45×10^3	–	–	2.00	–
EVA	2.09×10^3	9.60×10^2	–	–	3.11×10^{-1}	–
Silicon	2.09×10^3	2.33×10^3	–	–	1.30×10^2	–
TPT	1.25×10^3	1.20×10^3	–	–	1.50×10^{-1}	–
Vapor	1874	$Ideal\,gas\,\rho_v = \dfrac{p}{R_s T}$	–	–	0.0188	8.9×10^{-6}
Water	4180	1000	–	–	0.61	–
Alumina	900	3900	–	–	27	–
Bi_2Te_3 (p-n types)	154	7700	$\pm S(T)$ Table 1	$\sigma(T)$ Table 1	$k(T)$ Table 1	–
Copper	385	8960	–	58,100,000	400	–

3 Numerical model

The models used to describe the operation of the PV, TEG, Flat plate heat pipe and hybrid PV-TE are described in this section. Each of the subsystems are modelled individually firstly before being integrated into the hybrid system.

3.1 Photovoltaic model

The governing equations for the temperature distribution in each layer of the PV are given as [30]:

$$\rho C_p \frac{\partial T}{\partial t} - \nabla \cdot (k\nabla T) = \dot{q}_{sol} - \dot{P}_{gen} \tag{1}$$

where ρ, C_p and k are density, specific heat capacity and thermal conductivity of each layer. T is the temperature, $\dot{q}_{sol}$ can be defined as the volumetric solar energy absorption by each layer and $\dot{P}_{gen}$ is the electrical power generation per volume which is zero for all layers except the polycrystalline silicon cell layer.

The solar energy absorption and power generation in each layer of the PV can be modelled by firstly specifying the solar radiation intensity (G_0), after which the energy absorption in each layer can then be calculated and considered as an internal heat generation. In this study, the cell surface is assumed to always be uniformly illuminated. The volumetric energy absorption of each layer is given as:

$$\dot{q}_{sol,i} = \frac{G_{rec,i} \times \alpha_i \times A_i \times C}{V_i} \tag{2}$$

$$G_{rec,i} = G_{rec,i-1} \times \left[\left(1 - \alpha_{i-1} \right) - \rho_{i-1} \right] \tag{3}$$

where α_i, ρ_i and v_i are the absorptivity, reflectivity and volume of the ith layer respectively. $G_{rec,i}$ can be defined as the solar radiation intensity received at each layer, $\dot{q}_{sol,i}$ is the associated volumetric heat source at each layer, A_i is the area of the ith layer and c is solar concentration ratio.

In the polycrystalline silicon layer, power generation is considered as an internal heat sink and can be defined as [33]:

$$\eta_{pv} = \eta_{ref} \left[1 - \beta \left(T_c - T_{ref} \right) \right] \tag{4}$$

$$\dot{P}_{gen} = \dot{q}_{sol,si} \times \eta_{pv} \tag{5}$$

where η_{ref} is the reference efficiency of the polycrystalline silicon solar cell and β is the temperature coefficient. In addition, T_c is the average temperature of the silicon layer, T_{ref} is the reference temperature of 298.15 K and η_{pv} is the efficiency of the PV.

The electrical power generation obtained from Eq. (5) is dependent entirely on the temperature distribution in each of the layers therefore, Eqs. (1)–(5) are coupled together and solved simultaneously to obtain the temperature distribution using finite element method.

3.1.1 Boundary conditions

To accurately model the PV, the following boundary conditions are applied, and some assumptions are considered to simplify the model with minimal deviation from the real case.

a) Solar cell conversion efficiency at 298.15 K is assumed to be 17% and temperature coefficient to be 0.0045 K^{-1} [34].

b) Steady state conditions are assumed.

c) All layers are assumed to be of equal area and in direct contact.

d) Heat loss via convection and radiation are considered at the upper surface (glass) and back surface (tedlar) of the PV.

e) Thermal properties of all materials are assumed to be isotropic and constant.

f) Ambient temperature is equal on all sides of the PV and adiabatic condition is assumed.

g) Convective heat transfer at the back surface of the PV is assumed to be half of that of the front surface [35].

h) In terms of radiative heat loss, the front and back surface of the PV are taken to view the sky and ground respectively.

The sky temperature used for the radiative heat loss calculation at the surface of the PV is given as [34]:

$$T_{sky} = T_a - 6 (\text{K}) \tag{6}$$

where T_{sky} is sky temperature and T_a is ambient temperature.

The convective heat transfer coefficient of the PV is given in terms of the wind speed as [36]:

$$h = 5.82 + 4.07 v \tag{7}$$

where h is the convective heat transfer coefficient v is the wind speed (m/s).

3.2 Thermoelectric generator model

The governing equations for the TEG which are solved by using COMSOL 5.4 Multiphysics software are given as [37]:

$$\rho C_p \frac{\partial T}{\partial t} + \nabla \bullet \vec{q} = \dot{q} \tag{8}$$

where ρ is the density, C_p is specific heat capacity, T is temperature, $\vec{q}$ is heat flux vector and $\dot{q}$ is the heat generation rate per unit volume.

The electric charge continuity equation is given as [38],

$$\nabla \bullet \left(\vec{J} + \frac{\partial \vec{D}}{\partial t} \right) = 0 \qquad (9)$$

where $\vec{J}$ is the electric current density vector and $\vec{D}$ is the electric flux density vector.

Eqs. (5) and (6) are coupled using the following thermoelectric constitutive equations [39],

$$\vec{q} = T[\alpha] \bullet \vec{J} - [\kappa] \bullet \nabla T \qquad (10)$$

$$\vec{J} = [\sigma] \bullet (\vec{E} - [\alpha] \bullet \nabla T) \qquad (11)$$

where $[\alpha]$ is the Seebeck coefficient matrix, $[\kappa]$ is the thermal conductivity matrix and $[\sigma]$ represents the electrical conductivity matrix.

$$\vec{E} = -\nabla \varphi \qquad (12)$$

where $\vec{E}$ represents the electric field intensity vector and φ is the electric scalar potential.

The coupled thermoelectric equations can be obtained by combining the above equations as,

$$\rho_d C_p \frac{\partial T}{\partial t} + \nabla \bullet \left(T[\alpha] \bullet \vec{J} \right) - \nabla \bullet ([\alpha] \bullet \nabla T) = \dot{q} \qquad (13)$$

$$\nabla \bullet \left([\varepsilon] \bullet \nabla \frac{\partial \varphi}{\partial t} \right) + \nabla \bullet ([\sigma] \bullet [\alpha] \bullet \nabla T) + \nabla \bullet ([\sigma] \bullet \nabla \varphi) = 0 \qquad (14)$$

where $[\varepsilon]$ represents the dielectric permittivity matrix.

Lastly, the coupled thermoelectric governing equations can rewritten as [40],

$$\nabla \bullet \left(T\alpha \vec{J} \right) - \nabla \bullet (\lambda \nabla T) = \dot{q} \qquad (15)$$

$$\nabla \bullet (\sigma \alpha \nabla T) + \nabla \bullet (\sigma \nabla \varphi) = 0 \qquad (16)$$

The electrical performance of the TEG can be obtained from the following equations [8]:

$$V_{OC} = \alpha \Delta T \qquad (17)$$

where V_{OC} is the open circuit voltage, α is the Seebeck coefficient and $\Delta T = T_h - T_C$ is the temperature difference between the hot side and cold side of the thermoelectric generator.

$$V_L = V_{OC} - R_{in}I = R_L I \qquad (18)$$

Wwhere V_L is the output load voltage, R_{in} is the internal resistance of the TEG and I is the TEG current which is given as,

$$I = \frac{V_{OC}}{R_{in} + R_L} = \frac{\alpha \Delta T}{R_{in} + R_L} \qquad (19)$$

The output power of the TEG (P_{teg}) is given as,

$$P_{teg} = V_L I = R_L I^2 = \frac{R_L \bullet \alpha^2 \bullet \Delta T^2}{(R_{in} + R_L)^2} \qquad (20)$$

$$\eta_{teg} = P_{teg} \times Q_h \qquad (21)$$

where η_{teg} is the TEG efficiency and Q_h is the input heat flux at the top surface of the TEG.

3.2.1 Boundary conditions

a) Heat loss through convection and radiation on all surfaces of the TEG are assumed to be zero.

b) Electrical and thermal contact resistances are ignored.

c) The heat sink of the TEG is considered as a thermal boundary condition with a fixed temperature value.

d) The copper on the n-type thermoelectric leg is assumed to be at zero potential while the one at the p-type leg is connected to the external load resistance circuit.

3.3 Flat plate heat pipe model

The flat plate heat pipe model used in this study is a simplified model given by [41] and modified for this particular study.

The capillary pressure is given as:

$$\Delta p_c = \frac{2\sigma}{r_c} \tag{22}$$

where r_c is the capillary radius and σ is the surface tension.

The capillary pressure must be greater than all other pressure drops in the heat pipe therefore,

$$\Delta p_c \geq \Delta p_v + \Delta p_l + \Delta p_g \tag{23}$$

where Δp_v is the vapor pressure drop, Δp_c is capillary pressure drop, Δp_l is liquid pressure drop in wick and Δp_g is pressure drop due to gravitation and acceleration.

$$\Delta p_l = \left(\frac{\mu_l}{K A_w L_v p_l} \right) L_{eff} q \tag{24}$$

where μ_l is the liquid viscosity, κ is wick permeability, A_w is wick area, L_{eff} is the heat pipe effective length and q is the capillary limit.

The vapor pressure drop Δp_v can often be neglected and if the effect of gravity is not considered then,

$$\Delta p_c = \Delta p_l \tag{25}$$

The capillary limit is given as:

$$q = \frac{2\sigma K A_w L_v p_l}{L_{eff} r_c \mu_l} \tag{26}$$

$$L_{eff} = \frac{L_{evap}}{2} + \frac{L_{conden}}{2} \tag{27}$$

where L_{evap} is the length of evaporator section and L_{conden} is the length of condenser section of the heat pipe.

The effective thermal conductivity of the sintered copper powder wick is given as [41]:

$$k_{eff} = \frac{k_f \left(k_f + k_s - (1 - \varphi)(k_f - k_s) \right)}{k_f + k_s + (1 - \varphi)(k_f - k_s)} \tag{28}$$

where φ is porosity, taken as 0.5, k_f and k_s are thermal conductivity of fluid (water) and thermal conductivity of solid (copper) respectively, taken as 0.61 and 400 respectively.

The vapor density according to the Ideal gas law is given as:

$$\rho_v = \frac{p}{R_s T} = \frac{p \times M_n}{R_s T} \tag{29}$$

where p is pressure and M_n is the molar mass (18.01528 [g/mol]).

Laminar compressible flow is used and the saturation pressure (from Clausius-Clapeyron) at the inlet/outlet at evaporator/condenser side of the wick/vapor interface is given as:

$$p = p_{sat}(T) = p_{ref} \bullet exp \left(\frac{\lambda}{R_s} \left(\frac{1}{T_{ref}} - \frac{1}{T} \right) \right) \tag{30}$$

$$\lambda = h_{fg} \times M_n \tag{31}$$

where λ is the enthalpy of vaporization, M_n is the molar mass, h_{fg} is the latent heat (2473 [kJ/kg]), p_{sat} is saturation pressure, R_s is specific gas constant (8.3144621 [J/mol/K]), T_{ref} is reference temperature (100 °C), T is temperature and p_{ref} is reference pressure (1 atm).

A global analytical function is used to define the saturation pressure and the vapor density is calculated from the equation.

The resulting normal mass flux of the evaporating/condensing water at the wick/vapor interface is given as,

$$\dot{m} = \rho_v(\mathbf{v} \bullet \mathbf{n}) \tag{32}$$

where ρ_v is vapor density, v is velocity field component and n is normal direction.

Viscous dissipation is included in this model and heat conduction is present in the container and wick. In the vapor chamber, heat transfer is via conduction and convection.

The boundary heat source that accounts for the heat of evaporation/condensation at the wick/vapor interface is given as:

$$q_{evap} = \dot{m}\lambda \tag{33}$$

where $\dot{m}$ is normal mass flux and λ is the enthalpy of vaporization.

A global variable is used to define the heat of vaporization q_{evap} and a boundary heat source is used to apply it to the wick/vapor interface.

3.3.1 Boundary conditions

To accurately model the flat plate heat pipe, the following boundary conditions are applied, and some assumptions are considered to simplify the model [41].

a) Effect of gravity is neglected.

b) Heat transfer is mainly due to evaporation/condensation and convection of vapor. Therefore, heat transport in the wick is simplified as conduction with an effective heat transfer coefficient.

c) Constant material properties are used except for that of the vapor density.

d) This simplified model does not predict the operating limits of the heat pipe.

e) Convective heat transfer coefficient used at the top surface of the heat pipe is assumed to be 1200 W/m^2/K.

f) Sintered copper powder wick is used with porosity $\varphi = 0.5$.

3.4 Hybrid model

In this study, the model for the PV-TE and PV-TE-Heat pipe are essential the same because the heat pipe is simply a passive cooling device with no electrical contribution to the hybrid system. Instead, the heat pipe cools the PV thereby increasing the PV efficiency while also providing some heat flux at its condenser section for the TEG to generate electricity simultaneously.

The total power output of the hybrid system is a sum of the polycrystalline silicon cell layer power output and the TEG power output at matched load resistance. This is given as:

$$P_{total} = \dot{P}_{gen} + P_{teg} \tag{34}$$

Similarly, the overall efficiency of the hybrid system is given as the sum of the PV and TEG efficiencies.

$$\eta_{total} = \eta_{pv} + \eta_{teg} \tag{35}$$

3.5 Computational domain

The three-dimensional numerical simulations in this study are performed using COMSOL 5.4 Multiphysics software which is based on finite element method. The heat transfer in solid and liquid interface, laminar flow interface, electric current interface and electrical circuit interface are all used to perform the numerical study. Heat transfer in liquid is considered for the vapor chamber and boundary heat flux are used to describe the convective heat flux as appropriate. Domain heat source is used to describe the energy absorption in each of the PV layers and surface-to-ambient radiation interface is used to describe the radiative heat loss. In addition, a temperature boundary condition is applied to the TEG cold side and a porous medium interface is applied to the wick. In the laminar flow interface, an inlet boundary condition is set at the top surface of the vapor chamber with pressure set to the saturation pressure and normal flow direction is used. Furthermore, no slip wall condition is used. In all the simulation, the solar radiation intensity (G_0) is

1000 W/m^2 although, different concentration ratios are applied to increase this intensity. In addition, the inbuilt COMSOL PARDISO (Parallel Sparse Direct Solver) is used and a fully coupled direct linear solver is also used to perform the numerical study.

3.6 Model validation

Firstly, a mesh convergence test is performed to investigate the independency of the results on the mesh size. In built COMSOL physics-controlled mesh with different element size are used and the result is shown in Table 5 for the hybrid PV-TE-Heat pipe system considered. The average polycrystalline silicon cell temperature and overall hybrid system power output are obtained as shown in Table 5. It can be clearly seen that the average cell temperature and overall hybrid system power output converges when the Finer mesh is used. Therefore, for increased accuracy and to save computation time, the Finer mesh is used in all the simulations.

Table 5 Mesh convergence test.

Number of domain elements	Element size	Average cell temperature (K)	Overall hybrid power output (W)
70,269	Coarse	310.72	0.798606514
148,342	Normal	310.72	0.798597914
328,627	Fine	310.72	0.798587814
1,205,452	Finer	310.71	0.798598067
3,547,403	Extra fine	310.71	0.798598067

Secondly, to validate the model and numerical simulation methods used in this study, a comparison is made with previous works found in the literature. The PV model presented in [34] is used to validate the present PV model in this study. Simulation conditions are reset to those presented in [34] and the result is shown in Fig. 2a. The TEG model presented in [42] is used to validate the present TEG model used in this numerical simulations and the same conditions used are reset in this study for accurate comparison.

(a)

(b)
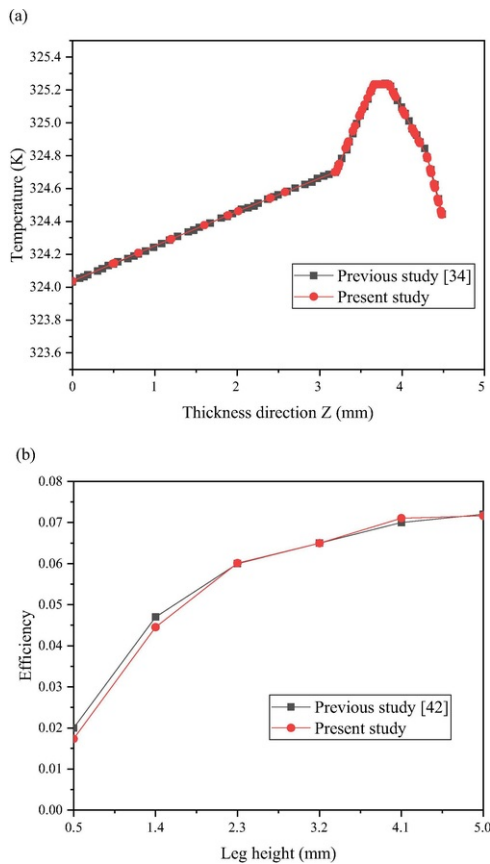
Fig. 2 Validation of (a) PV model with [34] and (b) TEG model with [42].

As can be seen from Fig. 2a and b, the numerical model developed in this study is in a very good agreement with previous models available in literature. The results are very identical therefore it can be concluded that the results obtained from this present study are accurate and justifiable. Lastly, the heat pipe model used in this study is the same model provided by COMSOL Multiphysics in their application gallery [41] therefore, there is no need to validate this model. However, it is important to know that the geometrical dimensions have been modified for the sake of this present study.

4 Results and discussion

In this section, the results obtained from this numerical study are presented and a detailed analysis of these results will be performed. The most important factors that influence the performance of the PV and hybrid PV-TE systems are analysed and a detailed comparison between the performance of the PV only, PV-TE and PV-TE-Heat pipe under the influence of varying solar concentration ratio, ambient temperature, wind speed and TEG cold side temperature is presented.

4.1 Influence of solar concentration ratio

Since the average solar radiation intensity (G_0) is kept constant all through this study, the solar concentration ratio is thus the determining factor for the total radiation impinged on the PV surface and absorbed by each later. Therefore, an increase in solar concentration ratio simply means an increase in radiation intensity since only uniform illumination is considered throughout this study. The influence of concentration ratio on the performance of the PV only, PV-TE and PV-TE-Heat pipe systems when the ambient temperature is 298.15 K and wind speed is 1 m/s is shown in Fig. 3. As expected, the efficiency of the systems decrease as the concentration ratio increases as shown in Fig. 3a. This is because, the increase in concentration ratio raises the temperature of the PV which in turn leads to a reduced overall efficiency in all the systems. However, it can be seen clearly from Fig. 3a that the PV-TE-Heat pipe system offers the highest conversion efficiency and slowest efficiency decline as the concentration ratio increases. In comparison, the efficiency of the PV only system shows a sharp decline as the concentration ratio increases. This can be attributed to the poor natural cooling of the PV only. On the other hand, the heat pipe provides a better and more efficient passive cooling of the PV thereby offering

an increased overall efficiency. The advantage of the PV-TE-Heat pipe system over the PV-TE and PV only systems becomes clearer as the concentration ratio increases. In fact, when the concentration ratio is 6, the PV-TE-Heat pipe efficiency is higher by 3.31% and 58.01% compared to that of the PV-TE and PV only systems respectively. Similarly, the maximum power output from the PV-TE-Heat pipe is enhanced by 1.31% and 57.23% compared to that of the PV-TE and PV only systems respectively when the concentration ratio is 6. Although the efficiency enhancement of the PV-TE-Heat pipe system compared to the PV-TE system is not much, it is important to note that the entire back surface of the PV is covered by the TEG in the PV-TE configuration. This is the only reason why the PV-TE system is efficient enough to compete with the PV-TE-Heat pipe system. However, in larger PV systems, the amount of TEG that will be required to cover the entire back surface of the PV will be a lot thus, the overall system cost will be high. This is where the PV-TE-Heat pipe system offers a superior advantage as the use of heat pipe can reduce the quantity of TEG needed to cool the PV. Furthermore, Fig. 3a shows that the PV-TE-Heat pipe system is better for highly concentrated system operation. It can also be seen from Fig. 3a that the power output of the PV only system first show a rising tendency after which it starts decreasing. This shows that there is an optimum concentration ratio for the PV only system. As seen from Fig. 3a, the optimum concentration ratio for maximum power output from the PV only system is 6. Fig. 3b shows the comparative performance of the PV in the PV only system, PV-TE and PV-TE-Heat pipe. It is obvious from Fig. 3b that the PV in PV-TE-Heat pipe possess the highest efficiency and power output due to the aforementioned cooling effectiveness of the heat pipe. Considering the efficiency and power output of the TE in the PV-TE and PV-TE-Heat pipe, Fig. 3c shows the comparative performance results obtained. One glaring observation is that the efficiency and power output of the TE in the PV-TE is significantly greater than that of the TE in PV-TE-Heat pipe. However, this is not surprising because the TE's performance is highly dependent on the amount of input heat flux into the system since both systems have the same cold side temperature. Therefore, the performance of the TE in PV-TE is significantly higher because there is a higher intensity of heat transferred from the PV to the TE due to the absence of any other cooling device behind the PV as is in the case of the PV-TE-Heat pipe. Moreover, the TE in the PV-TE-Heat pipe is attached to the condenser of the heat pipe which is at a much lower temperature. However, the contribution of the TE to the overall efficiency of the PV-TE and PV-TE-Heat pipe is not that significant because the PV contributes the greater share of the overall hybrid system efficiency. Consequently, the performance of the PV-TE-Heat pipe is still better than that of the PV-TE because the PV is better cooled.
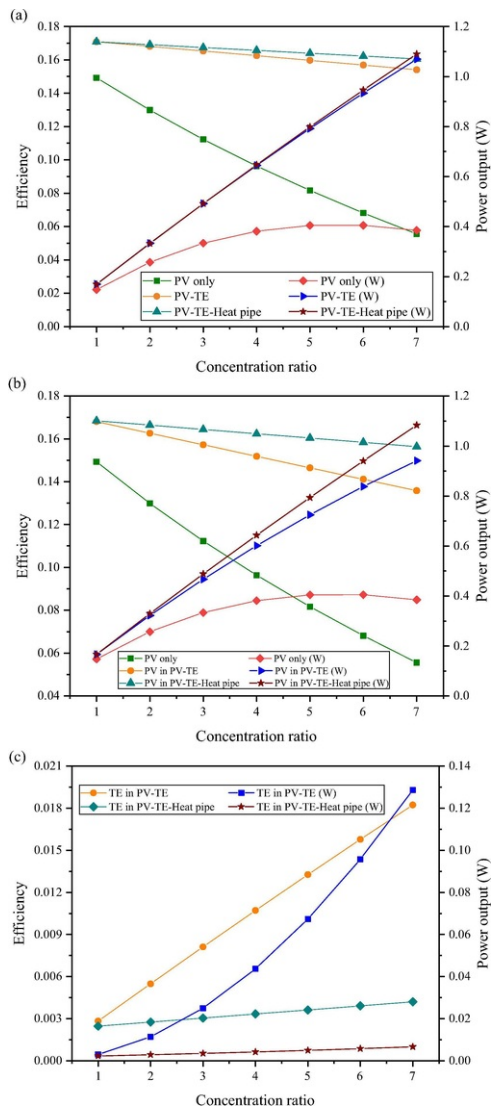
Fig. 3 Variation of concentration ratio with (a) overall (b) PV (c) TE efficiency and power output.

4.2 Influence of ambient temperature

The influence of the ambient temperature on the performance of the PV only and hybrid PV-TE systems when the concentration ratio is 6 and wind speed is 1 m/s is shown in Fig. 4. It can be seen from Fig. 4a that the efficiency and power output of the PV, PV-TE, PV-TE-Heat pipe all decrease as the ambient temperature increased. This trend is similar to the one reported in [25,26]. The reason for this is that the ambient temperature influences the amount of heat loss due to convection and radiation from the systems therefore, an increase in ambient temperature will ultimately lead to an increase in heat loss and a decrease in performance. Nevertheless, the PV-TE-Heat pipe still offers the best performance in that its efficiency is higher by 1.47% and 61.01% compared to that of the PV-TE and PV only systems at a high ambient temperature of 313.15 K. In addition, Fig. 4b shows the performance of the PV in the PV only, PV-TE and PV-TE-Heat pipe systems. It can be seen that the power output and efficiency of the PV decreases as the ambient temperature increased due to the heat losses to the environment. Furthermore, Fig. 4c shows the performance of the TE in the hybrid systems as the ambient temperature is varied. It can be seen that the power output and efficiency of the TE in the hybrid systems increase as the ambient temperature increase. This is because the increase in ambient temperature leads to a raise in the temperature of the PV therefore, the input heat flux to the TE is increased consequently, it's power output and efficiency is increased as shown in Fig. 4c.
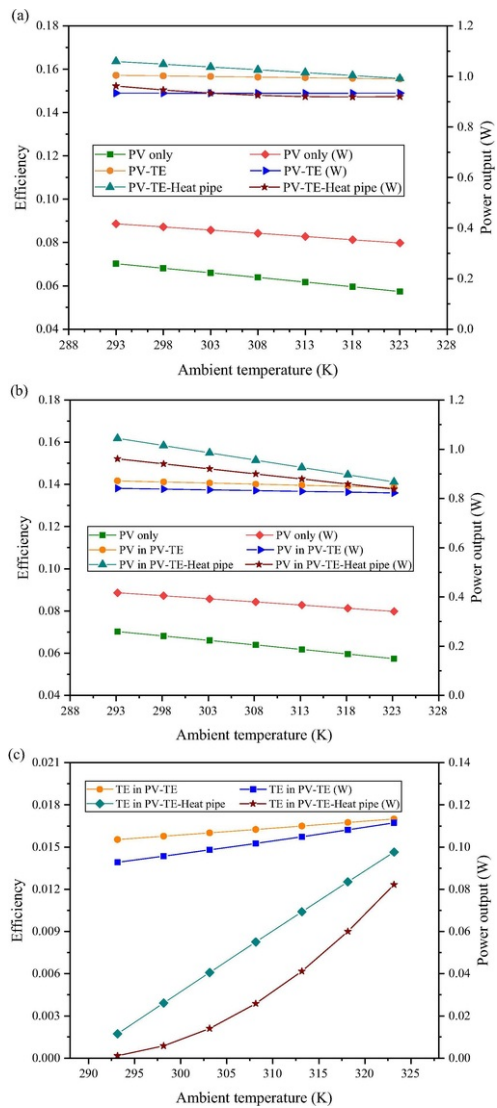
Fig. 4 Ambient temperature variation with (a) overall (b) PV (c) TE efficiency and power output.

4.3 Influence of wind speed

When the ambient temperature is 298.15 K and concentration ratio is 6, the influence of the wind speed on the performance of the PV only and hybrid PV-TE systems is shown in Fig. 5. It can be seen that an increase in wind speed leads to a rapid increase in the efficiency and power output of the PV only system and a slight increase in those of the hybrid systems. This is because the wind speed affects the convective heat transfer coefficient which accounts for the convective cooling of the PV therefore, an increase in wind speed ultimately leads to a decrease in PV temperature and an increase in performance. In addition, Fig. 5a shows that the PV-TE-Heat pipe performs better than the PV-TE and PV only systems. However, it can also be seen from Fig. 5a that the efficiency and power output increase offered by the PV-TE and PV-TE-Heat pipe as the wind speed increases is not that significant. This is because, unlike the PV only system in which natural convective cooling is applied to front and back surfaces of the PV, the PV-TE system only has convective cooling at the front surface of the PV due to the presence of TEG which covers the entire back surface of the PV. Similarly, the PV-TE-Heat pipe system also only has convective cooling at the front surface of the PV due to the presence of the heat pipe which covers the entire back surface of the PV. Therefore, the influence of the wind speed on the efficiency and power output of the PV-TE and PV-TE-Heat pipe is not that significant. In fact, the back surface of the PV-TE-Heat pipe is assumed to be insulated asides the TEG so as to

create sufficient temperature gradient for the TEG to operate. Fig. 5b shows the efficiency and power output varying of the PV in PV only, PV-TE and PV-TE-Heat pipe systems as the wind speed is increased. It can be seen clearly from Fig. 5b that the PV-TE performs better than the PV only although its performance is second only to that of the PV-TE-Heat pipe. Fig. 5c shows the performance of the TE in PV-TE and PV-TE-Heat pipe as the wind speed increases. It is obvious that the efficiency and power output of the TE in PV-TE decreases as the wind speed increases. This is due to the fact that an increase in wind speed leads to a better cooling of the PV and thus a reduced temperature and the input heat flux to the TE is reduced.
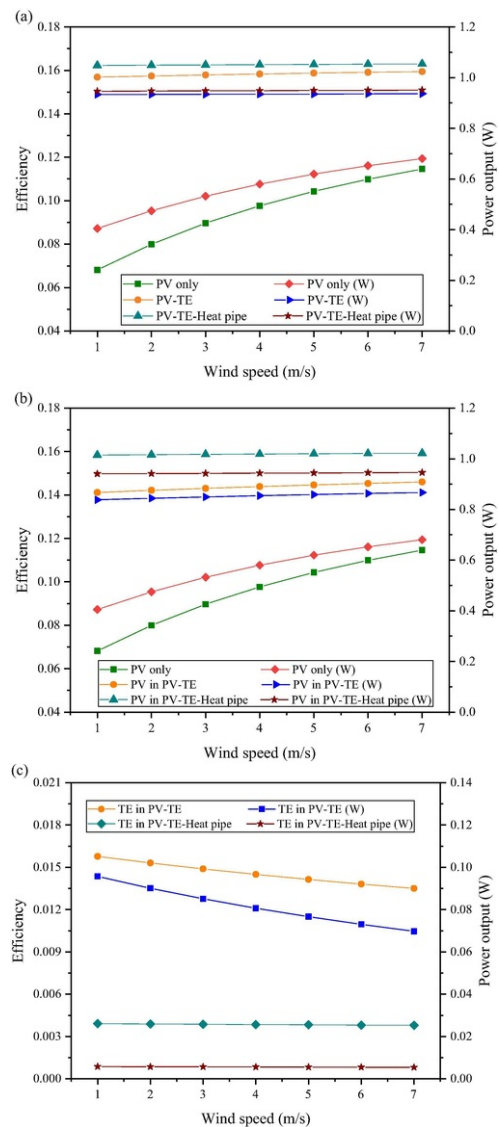
Fig. 5 Variation of wind speed with (a) overall (b) PV (c) TE efficiency and power output.

4.4 Influence of thermoelectric generator cold side temperature

Asides, the amount of input heat flux available to the TEG, the cooling effectiveness of the TEG is the other most important factor that influences the performance of the device. This is because, effective cooling at the cold side of the TEG creates a larger temperature difference across the TEG thus, more power can be generated. Fig. 6 shows the performance of the PV-TE and PV-TE-Heat pipe as the cold side temperature of the TEG is varied when the ambient temperature is 298.15 K, wind speed is 1 m/s and

concentration ratio is 6. It can be seen from Fig. 6a that the efficiency and power output of both hybrid PV-TE systems decrease as the TEG cold side temperature increased because the contribution of the TEG to the overall efficiency will decrease significantly due to the

lesser temperature difference available to the device. In addition, Fig. 6b shows that the power output and efficiency of the PV in PV-TE and PV-TE-Heat pipe decrease as the TEG cold side temperature increases because of the inadequate cooling provided. As expected,

Fig. 6c shows that the TE in PV-TE provide a better performance compared to the TE in PV-TE-Heat pipe because of the lesser temperature gradient. However, in both cases, the TE power output and efficiency sharply decrease as the TEG cold side temperature

increases thereby showing how highly important effective cooling of TEG is.
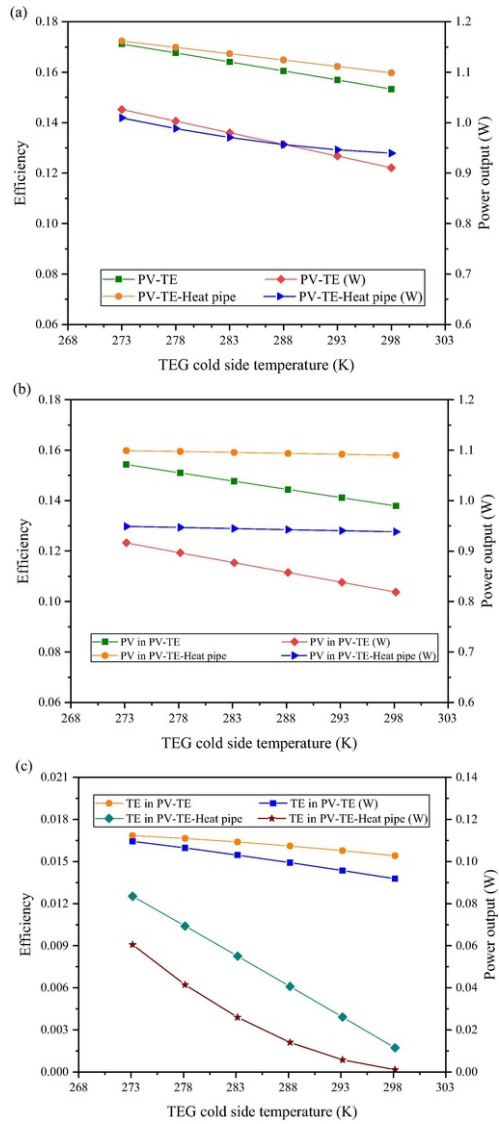
Fig. 6 TEG cold side temperature variation with (a) overall (b) PV (c) TE efficiency and power output.

4.5 Temperature and voltage distribution

Since it has been established that the TEG temperature gradient determines its performance, it is necessary to investigate the influence of ambient conditions on the thermoelectric generator temperature gradient. The variation of TEG temperature difference

with concentration ratio, ambient temperature, wind speed and TEG cold side temperature is shown in Fig. 7. It can be seen from Fig. 7a and b that TE temperature difference in PV-TE and PV-TE-Heat pipe increase as the concentration ratio and ambient temperature increases respectively. This trend is simply due to the fact that an increase in both the ambient temperature and concentration ratio leads to an increase in the input heat flux available to the TEG thus, its temperature difference increases. Contrarily, the TE temperature difference in PV-TE and PV-TE-Heat pipe decrease as the wind speed and TEG cold side temperature increases as shown in Fig. 7c and d respectively. Although for the wind speed, the temperature difference decrease is more visible in the PV-TE as shown in Fig. 7c. The reason for this is because an increase in wind speed leads to a decrease in PV temperature and consequently, a decrease in TE input heat flux. Similarly, an increase in the TEG cold side temperature leads to a decrease in the temperature gradient since the input heat flux is still constant.
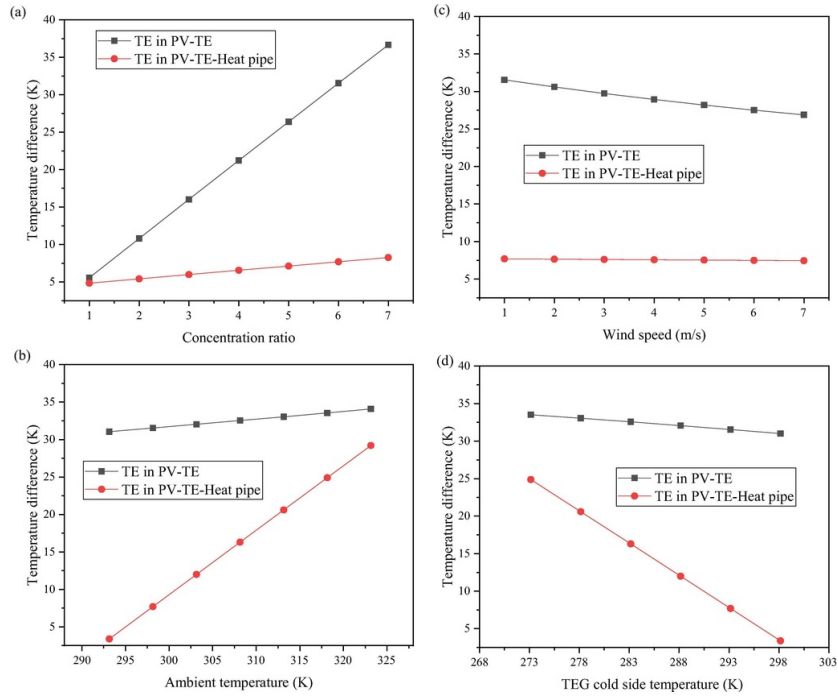
Fig. 7 Variation of TEG temperature difference with (a) concentration ratio (b) ambient temperature (c) wind speed (d) TEG cold side temperature.

The temperature and voltage distribution in the PV-TE are shown in Fig. 8 when ambient temperature is 298.15 K, wind speed is 1 m/s, concentration ratio is 6 and TEG cold side temperature is 293.15 K. The three-dimensional temperature distribution of the PV-TE can be seen from Fig. 8a. Under the aforementioned conditions, the maximum temperature in the PV-TE is 337 K. Fig. 8b shows the temperature distribution from the side view of the PV-TE while Fig. 8c shows the voltage distribution in the PV-TE. It can also be seen that the highest temperature in the hybrid PV-TE system is generated at the polycrystalline silicon layer.
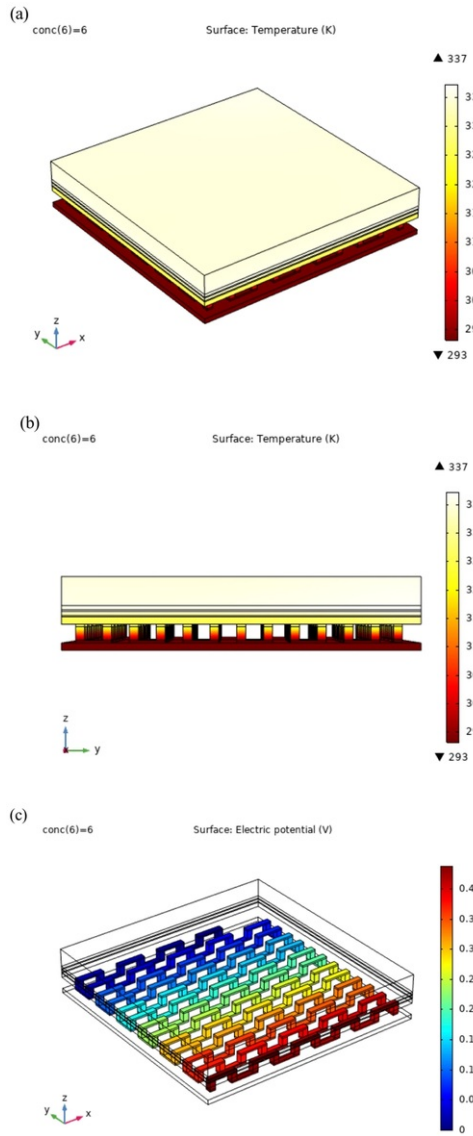
Fig. 8 PV-TE temperature distribution in (a) three-dimension (b) side view (c) voltage distribution.

Considering the PV-TE-Heat pipe, its temperature and voltage distribution are shown in Fig. 9 when ambient temperature is 298.15 K, wind speed is 1 m/s, concentration ratio is 6 and TEG cold side temperature is 293.15 K. Fig. 9a shows the three-dimensional temperature distribution of the PV-TE-Heat pipe. It can be seen clearly from Fig. 9a that the maximum temperature under the aforementioned conditions is 314 K which is 23 K lower than that in the PV-TE as shown in Fig. 8a. This shows the superiority of the flat plate heat pipe in cooling the PV compared to the TE. In addition, Fig. 9b shows the temperature distribution from the side view of the PV-TE-Heat pipe and it can be seen that the lowest temperature is from the TEG cold side. Finally, the TEG voltage distribution in the PV-TE-Heat pipe is shown in Fig. 9c. The thermoelectric legs are connected in series therefore, current flows across all the legs and voltage can be measure across the negative and positive terminals.
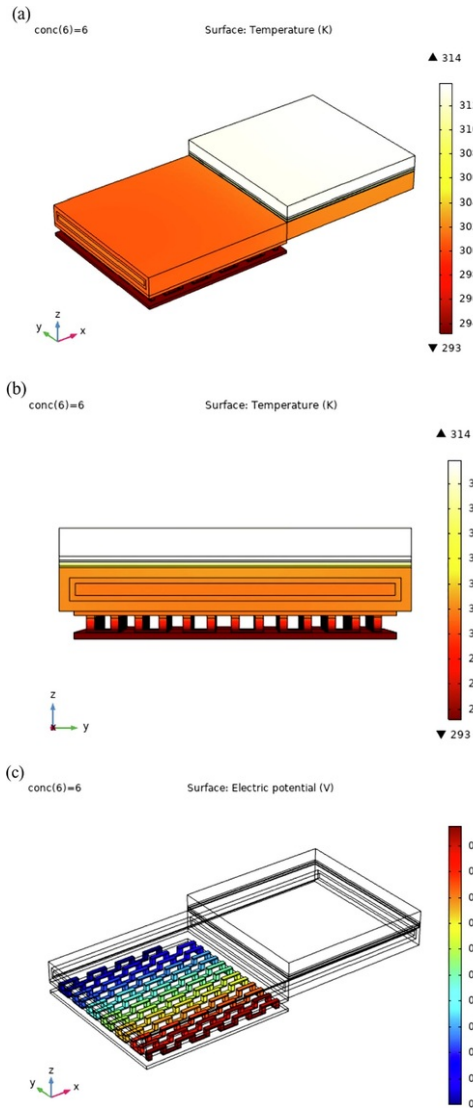
Fig. 9 PV-TE-Heat pipe temperature distribution in (a) three-dimension (b) side view (c) voltage distribution.

5 Conclusion

This study presented a detailed comparative analysis of the performance of a PV only, PV-TE and PV-TE-Heat pipe under varying ambient conditions. COMSOL 5.4 Multiphysics software which is based on the finite element method was used to perform the numerical simulations and three different models (PV, TEG, Heat pipe) for the hybrid system subsystems were developed and validated with data from available literature. A detailed literature review describing the current state-of-art in the field of hybrid photovoltaic-thermoelectric systems was presented to facilitate easy understanding of the subject matter and to justify the novelty of this study. For the first time, a three-dimensional numerical study of a hybrid photovoltaic-thermoelectric system employing a flat plate heat pipe was presented. Temperature dependent thermoelectric material properties were also accounted to increase the accuracy of the simulation results. The main conclusions from this study are as follows:

1) The PV-TE-Heat pipe system is recommended for highly concentrated systems because of its superior performance at high concentration ratios.

2) Efficiency of the PV-TE-Heat pipe is 3.31% and 58.01% higher compared to that of the PV-TE and PV only systems respectively at a concentration ratio of 6.

3) There exists an optimum concentration ratio for the maximum power output from the PV only system and it is 6.

4) Ambient temperature increase is not beneficial to the performance of the PV, PV-TE and PV-TE-Heat pipe. Nevertheless, the PV-TE-Heat pipe efficiency is 1.47% and 61.01% higher than that of the PV-TE and PV only systems at a high ambient temperature of 313.15 K.

5) Increase in wind speed enhances the performance of the PV, PV-TE and PV-TE-Heat pipe although the enhancement is not significant in the PV-TE and PV-TE-Heat pipe.

6) Although the PV-TE-Heat pipe system is recommended because of its superior performance, it is worth noting that the PV-TE system is also a better alternative to the PV only system because its performance is better compared to the PV only system.

7) The PV and TE have a complex relationship in that some ambient conditions are beneficial to the performance of the PV while harming that of the TEG and vice versa.

8) Ineffective cooling of the TEG could cause a negative effect on the performance of the hybrid systems.

Declaration of interests

The authors declare that they have no known competing financial interests or personal relationships that could have appeared to influence the work reported in this paper.

Acknowledgements

References

[1] M. Fisac, F.X. Villasevil and A.M. López, High-efficiency photovoltaic technology including thermoelectric generation, *J Power Sources* **252**, 2014, 264–269, https://doi.org/10.1016/j.jpowsour.2013.11.121.

[2] G. Li, S. Shittu, T.M.O. Diallo, M. Yu, X. Zhao and J. Ji, A review of solar photovoltaic-thermoelectric hybrid system for electricity generation, *Energy* **158**, 2018, 41–58, https://doi.org/10.1016/j.energy.2018.06.021.

[3] P. Huen and W.A. Daoud, Advances in hybrid solar photovoltaic and thermoelectric generators, *Renewable Sustainable Energy Rev* **72**, 2017, 1295–1302, https://doi.org/10.1016/j.rser.2016.10.042.

[4] T.M.O. Diallo, M. Yu, J. Zhou, X. Zhao, S. Shittu, G. Li, et al., Energy performance analysis of a novel solar PVT loop heat pipe employing a microchannel heat pipe evaporator and a PCM triple heat exchanger, *Energy* **167**, 2019, 866–888, https://doi.org/10.1016/j.energy.2018.10.192.

[5] A. Makki, S. Omer and H. Sabir, Advancements in hybrid photovoltaic systems for enhanced solar cells performance, *Renewable Sustainable Energy Rev* **41**, 2015, 658–684, https://doi.org/10.1016/j.rser.2014.08.069.

[6] X. Zhang, X. Zhao, S. Smith, J. Xu and X. Yu, Review of R & D progress and practical application of the solar photovoltaic/thermal (PV/T) technologies, *Renewable Sustainable Energy Rev* 2012, 599–617, https://doi.org/10.1016/j.rser.2011.08.026.

[7] M. Benghanem, A.A. Al-Mashraqi and K.O. Daffallah, Performance of solar cells using thermoelectric module in hot sites, *Renewable Energy* **89**, 2016, 51–59, https://doi.org/10.1016/j.renene.2015.12.011.

[8] S. Shittu, G. Li, X. Zhao, X. Ma, Y.G. Akhlaghi and E. Ayodele, High performance and thermal stress analysis of a segmented annular thermoelectric generator, *Energy Convers Manage* **184**, 2019, 180–193, https://doi.org/10.1016/j.enconman.2019.01.064.

[9] M. Zhang, L. Miao, Y.P. Kang, S. Tanemura, C.A.J. Fisher, G. Xu, et al., Efficient, low-cost solar thermoelectric cogenerators comprising evacuated tubular solar collectors and thermoelectric modules, *Appl Energy* **109**, 2013, 51–59, https://doi.org/10.1016/j.apenergy.2013.03.008.

[10] W. He, G. Zhang, X. Zhang, J. Ji, G. Li and X. Zhao, Recent development and application of thermoelectric generator and cooler, *Appl Energy* **143**, 2015, 1–25, https://doi.org/10.1016/j.apenergy.2014.12.075.

[11] H. Machrafi, Enhancement of a photovoltaic cell performance by a coupled cooled nanocomposite thermoelectric hybrid system, using extended thermodynamics, *Curr Appl Phys* **17**, 2017, 890–911, https://doi.org/10.1016/j.cap.2017.03.001.

[12] H. Hashim, J.J. Bomphrey and G. Min, Model for geometry optimisation of thermoelectric devices in a hybrid PV/TE system, *Renewable Energy* **87**, 2016, 458–463, https://doi.org/10.1016/j.renene.2015.10.029.

[13] F. Xin, T. Ma and Q. Wang, Thermal performance analysis of flat heat pipe with graded mini-grooves wick, *Appl Energy* **228**, 2018, 2129–2139, https://doi.org/10.1016/j.apenergy.2018.07.053.

[14] M.C. Zaghdoudi, S. Maalej, J. Mansouri and M.B.H. Sassi, Flat miniature heat pipes for electronics cooling: state of the art, experimental and theoretical analysis, *Int J Eng Appl Sci* **7**, 2011, 166–189.

[15] J. Qu and Q. Wang, Experimental study on the thermal performance of vertical closed-loop oscillating heat pipes and correlation modeling, *Appl Energy* **112**, 2013, 1154–1160, https://doi.org/10.1016/j.apenergy.2013.02.030.

[16] H. Jouhara, A. Chauhan, T. Nannou, S. Almahmoud, B. Delpech and L.C. Wrobel, Heat pipe based systems – advances and applications, *Energy* **128**, 2017, 729–754, https://doi.org/10.1016/j.energy.2017.04.028.

[17] X. Ju, Z. Wang, G. Flamant, P. Li and W. Zhao, Numerical analysis and optimization of a spectrum splitting concentration photovoltaic-thermoelectric hybrid system, *Sol Energy* **86**, 2012, 1941–1954, https://doi.org/10.1016/j.solener.2012.02.024.

[18] E. Yin, Q. Li and Y. Xuan, A novel optimal design method for concentration spectrum splitting photovoltaic thermoelectric hybrid system, *Energy* **163**, 2018, 519–532, https://doi.org/10.1016/j.apenergy.2018.05.127.

[19] W.G.J.H.M. Van Sark, Feasibility of photovoltaic – thermoelectric hybrid modules, *Appl Energy* **88**, 2011, 2785–2790, https://doi.org/10.1016/j.apenergy.2011.02.008.

[20] G. Li, K. Zhou, Z. Song, X. Zhao and J. Ji, Inconsistent phenomenon of thermoelectric load resistance for photovoltaic–thermoelectric module, *Energy Convers Manage* **161**, 2018, 155–161, https://doi.org/10.1016/j.enconman.2018.01.079.

[21] J. Zhang and Y. Xuan, An integrated design of the photovoltaic-thermoelectric hybrid system, *Sol Energy* **177**, 2019, 293–298, https://doi.org/10.1016/j.solener.2018.11.012.

[22] A. Lekbir, M. Meddad, A. Eddiai, S. Benhadouga and R. Khenfer, Higher-efficiency for combined photovoltaic-thermoelectric solar power generation, *Int J Green Energy* 2019, 1–7, https://doi.org/10.1080/15435075.2019.1567515.

[23] P.M. Rodrigo, A. Valera, E.F. Fernández and F.M. Almonacid, Performance and economic limits of passively cooled hybrid thermoelectric generator-concentrator photovoltaic modules, *Appl Energy* **238**, 2019, 1150–1162, https://doi.org/10.1016/J.APENERGY.2019.01.132.

[24] S. Mahmoudinezhad, S.A. Atouei, P.A. Cotfas, D.T. Cotfas, L.A. Rosendahl and A. Rezania, Experimental and numerical study on the transient behavior of multi- junction solar cell-thermoelectric generator hybrid system, *Energy Convers Manage* **184**, 2019, 448–455, https://doi.org/10.1016/j.enconman.2019.01.081.

[25] A. Makki, S. Omer, Y. Su and H. Sabir, Numerical investigation of heat pipe-based photovoltaic-thermoelectric generator (HP-PV/TEG) hybrid system, *Energy Convers Manage* **112**, 2016, 274–287, https://doi.org/10.1016/j.enconman.2015.12.069.

[26] G. Li, X. Zhao and J. Ji, Conceptual development of a novel photovoltaic-thermoelectric system and preliminary economic analysis, *Energy Convers Manage* **126**, 2016, 935–943, https://doi.org/10.1016/j.enconman.2016.08.074.

[27] G. Li, X. Zhao, Y. Jin, X. Chen, J. Ji and S. Shittu, Performance analysis and discussion on the thermoelectric element footprint for PV–TE maximum power generation, *J Electron Mater* **47**, 2018, 5344–5351, https://doi.org/10.1007/s11664-018-6421-4

[28] S. Shittu, G. Li, X. Zhao and X. Ma, Series of detail comparison and optimization of thermoelectric element geometry considering the PV effect, *Renewable Energy* **130**, 2019, 930–942, https://doi.org/10.1016/j.renene.2018.07.002.

[29] G. Li, S. Shittu, X. Ma and X. Zhao, Comparative analysis of thermoelectric elements optimum geometry between photovoltaic-thermoelectric and solar thermoelectric, *Energy* **171**, 2019, 599–610, https://doi.org/10.1016/j.energy.2019.01.057.

[30] H.R. Fallah Kohan, F. Lotfipour and M. Eslami, Numerical simulation of a photovoltaic thermoelectric hybrid power generation system, *Sol Energy* **174**, 2018, 537–548, https://doi.org/10.1016/j.solener.2018.09.046.

[31] F. Meng, L. Chen and F. Sun, Effects of temperature dependence of thermoelectric properties on the power and efficiency of a multielement thermoelectric generator, *Int J Energy Environ* **3**, 2012, 137–150.

[32] E. Skoplaki and J.A. Palyvos, On the temperature dependence of photovoltaic module electrical performance: a review of efficiency/power correlations, *Sol Energy* **83**, 2009, 614–624, https://doi.org/10.1016/j.solener.2008.10.008.

[33] D.L. Evans, Simplified method for predicting photovoltaic array output, *Sol Energy* **27**, 1981, 555–560.

[34] J.cheng Zhou, Z. Zhang, H.jian Liu and Q. Yi, Temperature distribution and back sheet role of polycrystalline silicon photovoltaic modules, *Appl Therm Eng* **111**, 2017, 1296–1303, https://doi.org/10.1016/j.applthermaleng.2016.10.095.

[35] Y. Lee and A.A.O. Tay, Finite element thermal analysis of a solar photovoltaic module, *Energy Procedia* **15**, 2012, 413–420, https://doi.org/10.1016/j.egypro.2012.02.050.

[36] J. Zhou, Q. Yi, Y. Wang and Z. Ye, Temperature distribution of photovoltaic module based on finite element simulation, *Sol Energy* **111**, 2015, 97–103, https://doi.org/10.1016/j.solener.2014.10.040.

[37] J. Xiao, T. Yang, P. Li, P. Zhai and Q. Zhang, Thermal design and management for performance optimization of solar thermoelectric generator, *Appl Energy* **93**, 2012, 33–38, https://doi.org/10.1016/j.apenergy.2011.06.006.

[38] H. Machrafi, An extended thermodynamic model for size-dependent thermoelectric properties at nanometric scales: application to nanofilms, nanocomposites and thin nanocomposite films, *Appl Math Model* **40**, 2016, 2143–2160, https://doi.org/10.1016/j.apm.2015.09.044.

[39] Antonova EE, Looman DC. Finite elements for thermoelectric device analysis in ANSYS. In: ICT 2005. 24th International Conf. Thermoelectr., 2005, p. 200–3. doi:10.1109/ICT.2005.1519922.

[40] M.A. Ezzat, Theory of fractional order in generalized thermoelectric MHD, *Appl Math Model* **35**, 2011, 4965–4978, https://doi.org/10.1016/j.apm.2011.04.004.

[41] COMSOL Multiphysics. Flat Heat Pipe. Appl Gall 2018. https://uk.comsol.com/model/flat-heat-pipe-43841 (accessed February 13, 2019).

[42] J.-L. Gao, Q.-G. Du, X.-D. Zhang and X.-Q. Jiang, Thermal stress analysis and structure parameter selection for a Bi2Te3-based thermoelectric module, *J Electron Mater* **40**, 2011, 884–888, https://doi.org/10.1007/s11664-011-1611-3.

[43] E. Yin, Q. Li and Y. Xuan, Effect of non-uniform illumination on performance of solar thermoelectric generators, *Front Energy* **12**, 2018, 239–248, https://doi.org/10.1007/s11708-018-0533-7.

[44] R.O. Suzuki, K.O. Ito and S. Oki, Analysis of the performance of thermoelectric modules under concentrated radiation heat flux, *J Electron Mater* **45**, 2016, 1827–1835, https://doi.org/10.1007/s11664-015-4237-z.

Highlights

- Hybrid photovoltaic-thermoelectric systems with and without heat pipe are studied.

- Comparison of the photovoltaic only and hybrid photovoltaic systems is presented.

- Influence of concentration ratio, ambient temperature, wind speed is investigated.

- Three-dimensional numerical simulation using finite element method is presented.

Queries and Answers

Query: Your article is registered as a regular item and is being processed for inclusion in a regular issue of the journal. If this is NOT correct and your article belongs to a Special Issue/Collection please contact J.Shanmugam@elsevier.com immediately prior to returning your corrections.
Answer: Yes

Query: The author names have been tagged as given names and surnames (surnames are highlighted in teal color). Please confirm if they have been identified correctly.
Answer: Yes

Query: Have we correctly interpreted the following funding source(s) and country names you cited in your article: EU Marie Curie International incoming Fellowships Program, United Kingdom? EPSRC , United Kingdom? EPSRC, United Kingdom? Innovate UK, United Kingdom? /
Answer: Yes